Terahertz Pulse Imaging of *ex vivo* Basal Cell Carcinoma

Ruth M. Woodward,*† Vincent P. Wallace,* Richard J. Pye,‡ Bryan E. Cole,* Donald D. Arnone,* Edmund H. Linfield,† and Michael Pepper*†

*TeraView Limited, Cambridge Science Park, Cambridge, U.K., †Cavendish Laboratory, University of Cambridge, U.K., and ‡Department of Dermatology, Addenbrooke's Hospital, Cambridge, U.K.

Terahertz pulse imaging has been used for the first time to study basal cell carcinoma *ex vivo*, the most common form of skin cancer. This noninvasive technique uses part of the electromagnetic spectrum in the frequency range 0.1–2.7 THz. A total of 21 samples were imaged; the study was performed blind and results were compared to histology. Each image consisted of possible diseased tissue and normal tissue from the same patient. The diseased tissue showed an increase in absorption compared to normal tissue, which is attributed to either an increase in the interstitial water within the diseased tissue or a change in the vibrational modes of water molecules with other functional groups. Seventeen of the images showed a significant difference between the normal and the diseased tissue. These were confirmed by histology to be basal cell carcinomas. Of the remaining four cases, three showed no contrast and were confirmed as blind controls of normal tissue; the fourth case was a suspected basal cell carcinoma but showed no contrast, and histology showed no tumor. Cross-sections of the terahertz images, showing the terahertz absorption, were compared to histology. Regions of increased terahertz absorption agreed well with the location of the tumor sites. Resolutions at 1 THz of 350 μm laterally and 40 μm axially in skin were attainable with our system. These results demonstrate the ability of terahertz pulse imaging to distinguish basal cell carcinoma from normal tissue, and this macroscopic technique may, in the future, help plan surgery.
Key words: biopsy/imaging/micrographic surgery/Mohs/skin cancer. J Invest Dermatol 120:72–78, 2003

Basal cell carcinoma (BCC) is the most common form of cancer worldwide in white populations and has a reported annual incidence of over 1 million in the U.S.A. (American Cancer Society, 2001); in the U.K. the incidence rate has increased by 50% in the last 10 y (Holme *et al*, 2000). The diagnosis of BCC is based on visual assessment; where there is doubt a biopsy may be of value and this also provides information on the histologic subtype of the tumor (Telfer *et al*, 1999). For well-defined, solid, cystic, and superficial BCCs, and for tumors of less than 20 mm in diameter, surgical excision is the treatment of choice. A minimum margin of 4 mm is required to completely excise the tumor in more than 95% of cases (Wolf and Zitelli, 1987). Ill-defined, micronodular, infiltrating, and sclerosing tumors may extend 15 mm or more beyond the clinical edge. Accurate histology reflecting all the tumor margins seems to be essential to achieve cure. None of the reported range of histologic techniques used is ideal (Rapini, 1990), but Mohs' micrographic surgery (MMS) is probably the best as it allows review of all the margins and same-day closure of the defects (Shriner *et al*, 1998).

There are a number of advantages offered by MMS. Infiltrating, sclerotic tumors can be defined accurately and the direction of the tumor spread identified, thus conserving tissue and avoiding the need for a "blind" wide excision. High cure rates of 99% at 5 y in primary tumors and 96% in recurrent tumors are widely reported using this technique. MMS is time consuming and expensive, however. Any system that could help define the histologic subtype of the BCC and direction of subclinical spread preoperatively, without performing a biopsy, may simplify MMS to a single layer for all but the most extensive tumors.

Several different imaging techniques are being evaluated as diagnostic tools for skin lesions and tumor margin assessment. High frequency ultrasound is capable of visualizing tumor dimensions *in vivo* with axial and lateral resolutions of 80 μm and 200 μm, respectively, and a penetration depth of 7 mm (Hoffmann *et al*, 1990; Lassau *et al*, 1997). The technique does not have chemical specificity, however, and cannot differentiate between benign and malignant skin lesions, and so its role may be limited (Fornage *et al*, 1993; Hoffmann *et al*, 1999).

Magnetic resonance imaging usually only provides useful information when the tumor extends more than 15 mm below the surface (Heinritz *et al*, 1995). *In vivo* measurements on human skin using magnetic resonance microscopy with axial and lateral resolutions of 19 μm and 78 μm, respectively, and a penetration depth of 800 μm have been reported (Song *et al*, 1997). Problems associated with this technique, however, e.g., the use of a whole body imaging machine, high costs, system complexity, acquisition time, and patient claustrophobia, currently make it unsuitable for imaging skin cancer (Bushberg, 1994; Price, 1999).

Near infrared (NIR) imaging techniques (wavelength range 0.7–2 μm) include optical coherence tomography (OCT) and confocal microscopy. Both provide information about the structure of tissue at depth. OCT is capable of visualizing architectural changes in tissue at spatial resolutions of 10 μm, with a penetration

Manuscript received November 9, 2001; revised September 2, 2002; accepted for publication September 23, 2002

Reprint requests to: Vincent P. Wallace, TeraView Limited, 302–304 Cambridge Science Park, Milton Road, Cambridge, CB4 0WG, U.K.

Abbreviations: BCC, basal cell carcinoma; MMS, Mohs' micrographic surgery; NIR, near infrared; OCT, optical coherence tomography; TPI, terahertz pulse imaging; TPP, time post pulse.

depth of less than 1 mm (Schmitt *et al*, 1995). It is very difficult to differentiate inflammatory processes, cancer, and scarring, however, using OCT (Kuranov *et al*, 2002). Confocal microscopy is a high resolution, real-time imaging technique, able to visualize cellular and nuclear detail *in vivo*, at lateral and axial resolutions of 1–2 μm and 3–5 μm, respectively, with a penetration depth of 250–300 μm (Rajadhyaksha *et al*, 1995; Rajadhyaksha and Zavislan, 1998; Huzaira *et al*, 2001). The current small field of view, 250 × 250 μm, prevents macroscopic visualization of tumor margins, but by tiling individual frames to form a mosaic, larger fields can be viewed *ex vivo* (Rajadhyaksha *et al*, 2001). NIR light is highly scattered by tissue structures on a similar scale as the wavelengths used, e.g., cells, membranes, nuclei, and collagen. Both of these NIR techniques rely on backscattered photons to form images. Therefore, a major limitation of these techniques is the poor penetration due to loss of signal after a few hundred microns. Scattering of light by tissue is less of a problem at longer wavelengths.

The terahertz (THz) gap, typically defined as the frequency range 0.1–10 THz, corresponding to a wavelength range of 3 mm to 30 μm, was a previously unexplored region of the electromagnetic spectrum, owing to a lack of suitable sources and detectors (Arnone *et al*, 1999; Cole *et al*, 2001). This frequency range is of particular interest as it excites the intermolecular interactions, such as the librational and vibrational modes of molecules (Zelsmann, 1995), providing spectroscopic information.

Terahertz pulse imaging (TPI) is a noninvasive, coherent optical imaging modality that explores this frequency region and has a current usable range of 0.1–2.7 THz, 3 mm to 110 μm in wavelength. These wavelengths are significantly larger than the scattering structures in tissue; therefore we assume that scattering effects are negligible. The current lateral and axial resolutions attainable with our system at 1 THz are 350 μm and 40 μm, respectively, making it a viable imaging modality. As TPI is a coherent, time gated, low noise technique, both phase and amplitude information can be obtained, from which the absorption and refractive index of a medium can be determined. This enables TPI to provide both structural and functional information, due to chemical specificity. Through examination of the terahertz waveform in both the time and frequency domains, TPI may prove advantageous in distinguishing type, lateral spread, and depth of tumors.

The purpose of this study was to determine whether TPI could differentiate between BCC and normal tissue and to test whether it can help with the demarcation of BCC margins prior to MMS. Twenty-one samples were analyzed and time-domain analysis techniques were used to produce the two-dimensional terahertz images. Terahertz cross-sections of the diseased tissue were then compared to histology to determine whether the increase in the terahertz absorption observed correlated with the location of the tumor sites.

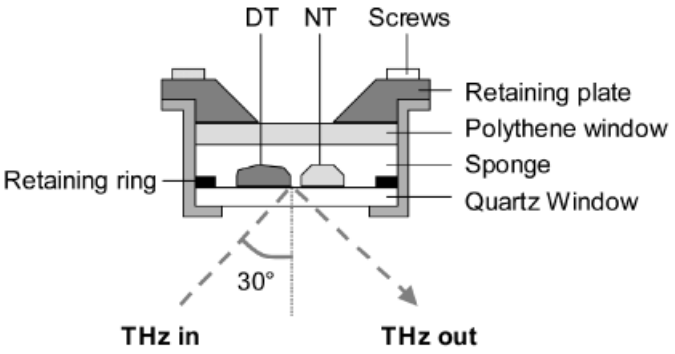

Figure 1. Sample holder. Cross-sectional schematic of sample holder. DT – diseased tissue, NT – normal tissue. Tissue is placed directly on the quartz window.

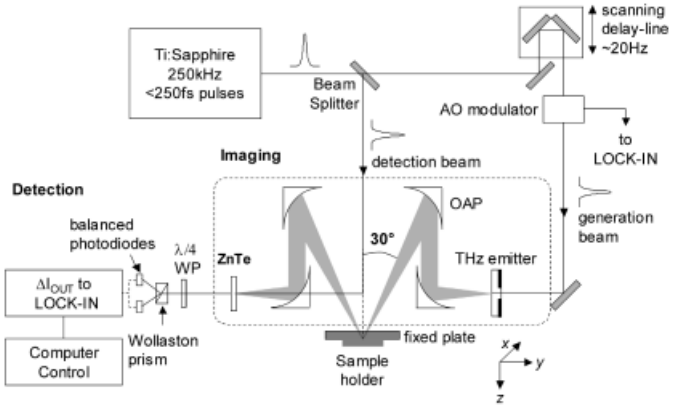

Figure 2. Terahertz Pulse Imaging (TPI) system. Schematic diagram of the TPI system in reflection geometry. AO – acousto-optic modulator; OAP – off-axis parabolic mirrors; ZnTe – zinc telluride; WP–λ/4 quarter waveplate; ΔI_{OUT} – difference in output current from balanced photodiodes. The THz optics, which are scanned in the *x*–*y* plane, are marked by the dashed box. The sample holder is placed on the fixed plate.

MATERIALS AND METHODS

Tissue preparation Excised skin tissue was obtained from the Department of Dermatology at Addenbrooke's Hospital, Cambridge, U.K. All patients (aged 29–77, mean age 60±13 y; 13 males and eight females) were undergoing MMS for clinically ill-defined, incompletely excised, or recurrent BCCs. Obvious tumor was removed prior to the first layer of MMS and sent for TPI. Excess normal skin was obtained during reconstruction and was located close to the tumor site. All tissue, including the normal skin, was stored in keratinocyte culture medium (Gibco BRL Keratinocyte-SFM, Life Technologies, Scotland), refrigerated at 4°C, and imaged within 10 d of excision. Keratinocyte culture medium was chosen as it was felt least likely to alter the skin tissue. Appropriate consent was obtained for the study; all patient material was made anonymous and returned to Addenbrooke's Hospital for histology or disposal.

The study was performed blind. A sample consisted of a piece of suspected BCC and normal tissue, taken from the same patient. Prior to imaging, excess fluid was removed from the skin samples using lint-free paper. The diseased and normal tissue were placed side by side, inside the sample holder, as shown in **Fig 1**. The skin was placed in direct contact with the quartz window (diameter 25 mm, thickness 2 mm), with the top surface of the skin facing the incident terahertz radiation. No immersion medium was used between the quartz window and the tissue, and air gaps were minimized. A small piece of sponge held the tissue in place and flat against the window. A retaining ring was placed on the window to prevent tissue movement and provide a level platform for the polythene disc, which was placed on top of the sponge and secured by a retaining plate. This airtight holder prevented the tissue from drying out during imaging. After imaging, the tissue was photographed, removed from the sample holder, placed in formalin, and submitted for routine histology.

TPI system The TPI system used reflection geometry, as shown in **Fig 2**. Optical excitation was achieved using a Ti:sapphire laser (RegA 9000, Coherent, CA) emitting 250 fs pulses centered at a wavelength of 800 nm, with a 250 kHz repetition rate. A 50:50 beamsplitter separated the pulses into two beams, an excitation beam and a detection beam. Generation of the terahertz was achieved by optical excitation of a gallium arsenide wide aperture (1 mm) antenna, biased at 1 kV (Van Exter and Grischkowsky, 1990). This gave a usable frequency range of 0.1–2.7 THz with an average power of approximately 1 mW (Cole *et al*, 2001).

The terahertz pulses were collimated and focused onto the tissue by a pair of off-axis parabolic (OAP) mirrors. The sample holder was mounted on a fixed plate, as indicated in **Fig 2**. The angle of reflection was 30° to the normal. The terahertz pulses reflected from the tissue were re-collimated using another pair of OAP mirrors and focused onto a 1 mm thick zinc telluride crystal, collinear with the detection beam. Detection was achieved using electro-optic sampling (Wu and Zhang, 1995), as indicated in **Fig 2**. In the presence of terahertz radiation, birefringence is induced in the zinc telluride crystal, which causes a change in polarization of the detection beam from circular to elliptical. A polarizer, quarter waveplate,

and Wollaston prism separate the two orthogonal states, and the change in polarization is detected by the balanced photodiodes. In the presence of terahertz radiation a nonzero output current ΔI_{OUT} results (**Fig 2**). As the effect is linear and instantaneous the output current is directly proportional to the terahertz electric field. To improve the sensitivity, the generation beam was chopped with an acousto-optic modulator so that lock-in techniques could be used. By sweeping the optical delay through the entire terahertz pulse at a rate of 20 Hz, the time-domain terahertz waveforms were obtained. The frequency-domain spectra were retrieved using fast Fourier transforms. The entire terahertz optics, indicated by the dashed box (**Fig 2**), were raster-scanned in the x–y plane to form an image.

To remove any system response, the raw terahertz waveform of the tissue at each pixel was divided by a reference waveform in the frequency domain and a numerical bandpass filter was applied to remove high and low frequency noise. The resultant deconvolved waveform and the raw terahertz waveform of skin tissue, in the time domain, are shown in **Fig 3**.

The system had a lateral resolution of 130 μm to 3.7 mm over the wavelength range of 110 μm to 3 mm, which, in the far-field scanning plane, is diffraction limited. The time resolution of 0.5 ps was limited by the laser pulse duration; assuming a refractive index of 4 in skin tissue in this frequency range, an axial resolution of approximately 40 μm close to the skin surface can be achieved. To reduce any noise from laser fluctuations the waveform was averaged four times per pixel. The signal-to-noise ratio was approximately 6000:1. The time-domain waveform acquired information to a depth of the order of 1 mm into the skin samples (Cole *et al*, 2001), which was sufficient for tissue analysis. The maximum recorded energy incident on a skin sample, with a spot diameter of 350 μm using our 1 mW source, was 2×10^4 J per m^2, which takes into account the beam overlap in each pixel when scanning in the x–y plane. The average exposure time over all samples was 500 ms. The incident energy is over 1000 times lower than the maximum permissible exposure at similar frequencies (EN 60825–1, 1994). Cultured keratinocytes irradiated for longer times have shown no adverse change (Clothier, 2002); therefore we assume the skin samples are unaffected by the terahertz radiation.

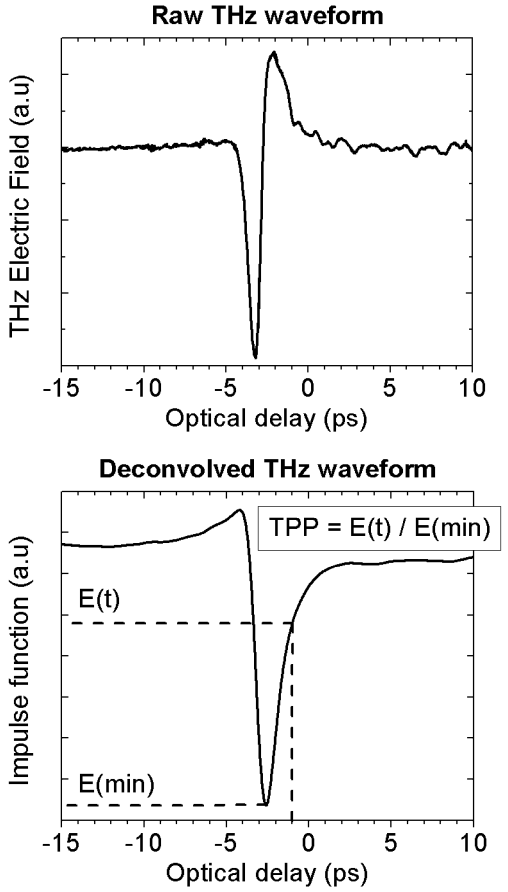

Figure 3. Raw and deconvolved THz waveforms. Typical THz waveforms of skin tissue in the time-domain for a single pixel. The deconvolved THz waveform shows the time post pulse (TPP) analysis technique, TPP = E(t)/E(min), where E(t) is the impulse function at time t and E(min) the minimum impulse function.

Data analysis and statistical methods The terahertz images were generated using an analysis technique called time post pulse (TPP), where TPP = $E(t)/E$(min), as shown in **Fig 3**. This method uses the deconvolved waveform at each pixel in the time domain. TPP normalizes the impulse function at a time t, $E(t)$, by the minimum peak value, E(min) (**Fig 3**). This time-domain analysis technique allows for the direct comparison of the relative change of terahertz waveforms and has been shown to differentiate between diseased and normal tissue (Woodward *et al*, 2002). As the terahertz pulse propagates through an absorptive medium, such as skin tissue, it broadens in time (Cole *et al*, 2001). The greater the absorption is, the greater the broadening of the terahertz pulse, which results in a larger TPP value.

The terahertz images in **Fig 4** were produced by plotting the TPP value at a particular time t at each pixel over the area scanned. Typically, t was chosen to provide the best contrast between the diseased and normal tissue. The mean and standard deviation of the TPP values were calculated for areas defined within the diseased (d1, d2) and normal (n1, n2) tissue regions marked by the solid boxes in the terahertz images of **Fig 4**, and are displayed by the histograms, also in **Fig 4**. A t test was performed between the diseased and normal areas to determine the statistical significance of the terahertz contrast observed between them (Barlow, 1989). If the TPP value in the suspected BCC was significantly greater than the normal skin tissue at the $p < 0.001$ level, the terahertz contrast was positive and the tissue was defined as diseased.

A suture placed on the edge of the BCC allowed orientation of the histology sections and acted as a reference point for both the visible and terahertz images. The histology cross-section was taken from the suture location through the center of the tumor, as indicated by the dotted white line on the visible images in **Fig 4**. A similar cross-section was taken through the terahertz images, and the TPP value was plotted as a function of distance from the suture location. This we define as the terahertz absorption profile. A comparison between the histology sections and the terahertz absorption profiles is shown in **Fig 5**.

RESULTS

Sample 1 is from a patient with a primary, clinically ill-defined BCC on the nasal bridge, 7 mm in diameter (**Fig 4*a***). The visible image shows an annular area of erythema in the diseased tissue, which is indicated by a solid boundary. The false color terahertz image shows a strong contrast between the diseased tissue (*solid boundary*), shown as yellow and red "hot spots", and the normal tissue (*dashed boundary*), which shows a uniform green color throughout. This contrast is not as evident in the visible image. In the histogram, the mean TPP values of the two diseased regions are significantly larger than those of the normal tissue. **Figure 5(*a*)** compares the histology section to the terahertz absorption profile, calculated by plotting the TPP value along the dotted white line marked in **Fig 4(*a*)**. The histology shows a nodular BCC, and the suture is indicated on the left with an X. The terahertz absorption profile shows a maximum in absorption 6 mm from the suture, indicating diseased tissue, which correlates well with location of the tumor in the histology section.

Sample 8 is from a patient with a primary, micronodular tumor 15 mm in diameter, located on the upper lip and involving the left portion of the philtrum (**Fig 4*b***). The visible image shows an area of erythema, located in the lower and lateral pole of the diseased tissue, but the remainder appears normal. The false color terahertz image exhibits contrast between the diseased and normal tissue. The tumor appears to extend beyond the region of inflammation seen clinically. An area of possibly normal tissue is also evident in the terahertz image amongst the tumor, indicated by a lighter, green circular region. The normal tissue shows uniform contrast throughout. The mean TPP values for the selected areas of diseased and normal tissue, displayed in the histogram, show statistically significant differences between the diseased and normal tissue, although the contrast is not as marked as in Sample 1. **Figure 5(*b*)** demonstrates the similarity between histology and the terahertz absorption profile. In the histology section, the scattered infiltrates of micronodular BCC are present close to the suture and a region of normal tissue is identified within the tumor.

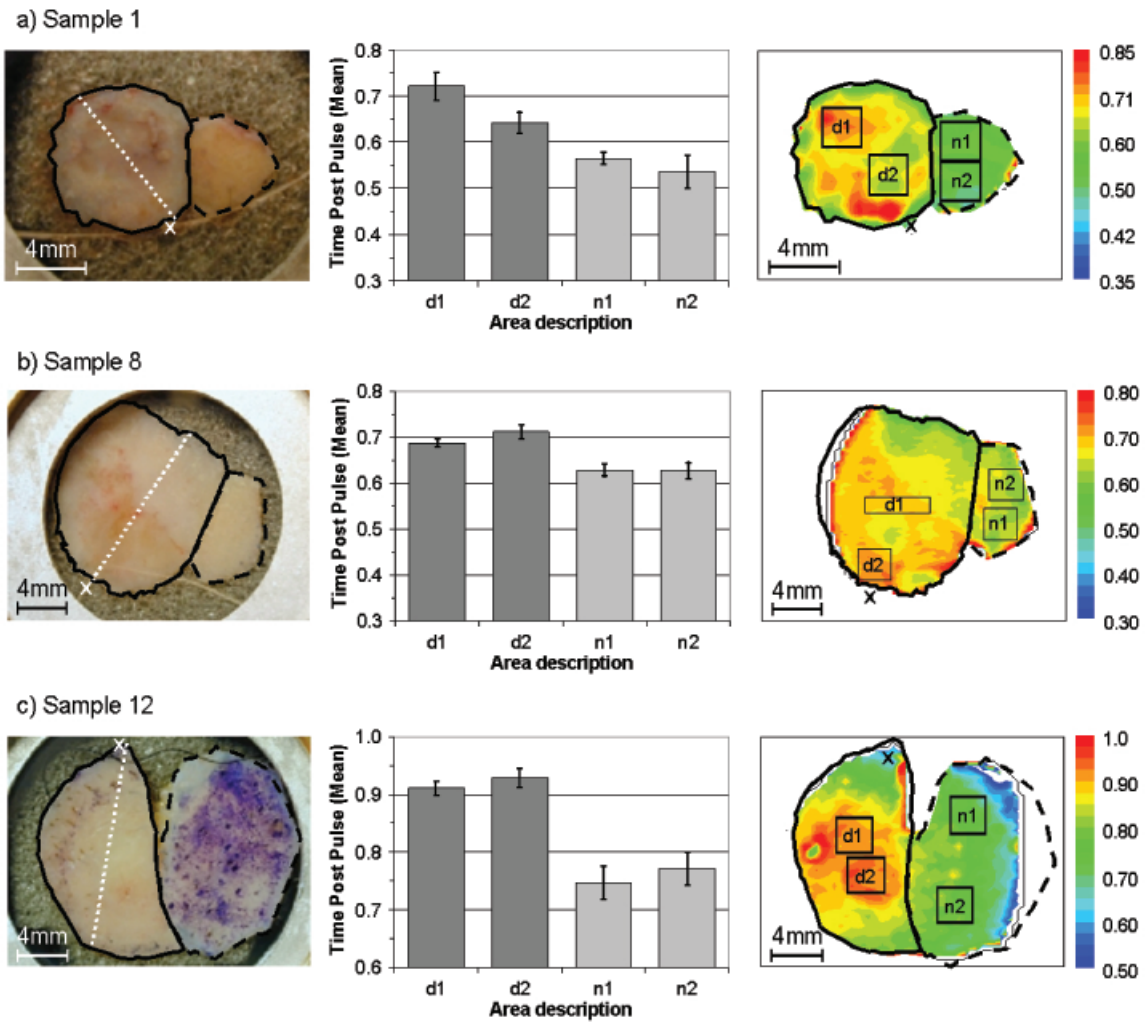

Figure 4. Visible and THz images. A comparison between the visible images, on the left, and the THz images, on the right, of samples 1, 8 and 12. The diseased tissue, on the left of the visible image, is marked by a solid boundary, the normal tissue on the right by a dashed boundary. The dotted white line indicates the axis of the vertical histology section. The white 'x' marks the location of the suture. The histograms show the mean TPP value, and the error bars its resultant standard deviation in the areas highlighted by the boxes in the THz images, in which 'x' marks the location of the suture. Equal size areas d1 and d2 were located on the diseased tissue, and n1 and n2 on the normal tissue.

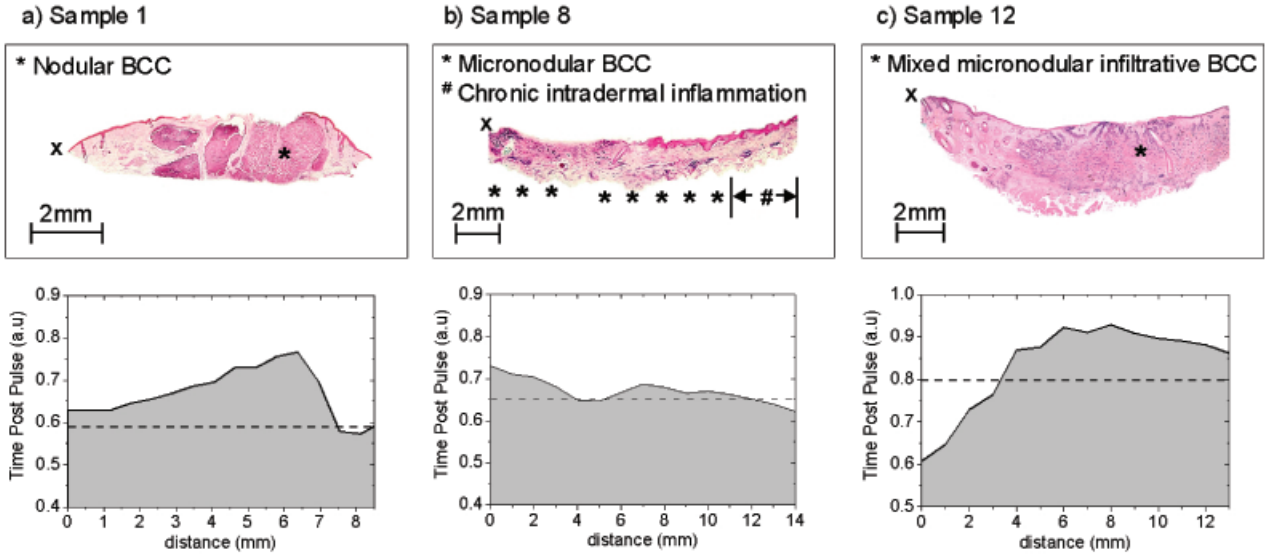

Figure 5. Histology sections and THz absorption profiles. In the vertical histology sections at the top of the figure, 'x' marks the location of the suture and * the tumour sites. In b), sample 8, the tumour sites are marked as they are difficult to locate histologically, #-chronic intradermal inflammation. The THz absorption profiles on the bottom of the figure, orientated to histology, show the TPP value along the white dotted lines marked in the visible images of **Figure 4**. The black dashed line marks the maximum TPP value including its standard deviation, from the histograms of **Figure 4**. Below the dashed black line the tissue is expected to be normal.

Table I. Results for all samples imaged within 10 d of excision

Patient (sample)	Age (y)	Sex[a]	Diseased area (mm^2)	Number of pixels in area	Site	Histologic subtype	Terahertz contrast
1	43	M	4.80	30	Nasal bridge	Infiltrative nodular	Diseased
2	57	F	9.18	80	Left ala	Infiltrative	Diseased
3	55	F	5.02	90	Nasal tip	Micronodular	Diseased
4	63	F	5.77	70	Nasal tip	Nodular	Diseased
5	64	F	11.31	120	Nasal tip	Recurrent infiltrative	Diseased
6	52	F	10.64	112	Forehead	Normal	Normal
7	64	M	7.98	84	Right ala	Infiltrative	Diseased
8	29	F	6.62	70	Left upper lip	Infiltrative micronodular	Diseased
9	39	M	15.50	168	Left side nose	Recurrent infiltrative	Diseased
10	63	M	19.05	40	Nasal tip	Normal	Normal
11	60	M	12.86	36	Right nasal tip	Infiltrative	Diseased
12	58	M	9.37	48	Central chin	Infiltrative	Diseased
13	66	F	15.61	80	Right lower lid	Infiltrative	Diseased
14	57	M	13.51	70	Left upper pinna	Infiltrative	Diseased
15	62	M	11.43	60	Left postauricular	Infiltrative	Diseased
16	76	M	22.87	120	Right preauricular	Normal	Normal
17	72	F	14.12	96	Nasal bridge	Infiltrative	Diseased
18	76	M	14.12	90	Right upper lip	Infiltrative	Diseased
19	46	M	6.59	42	Left ala	Morphoeic	Diseased
20	77	M	13.16	120	Nasal tip	Infiltrative	Diseased
21	77	M	13.16	120	Nasal tip	Normal	Normal

[a]M, male; F, female.

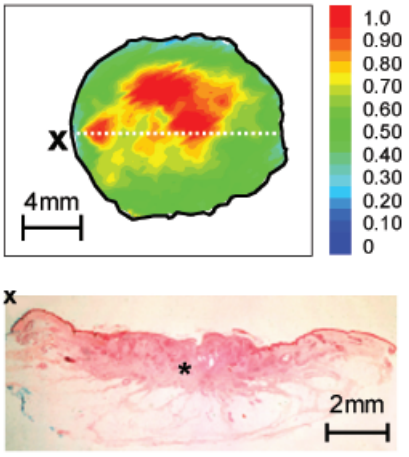

Figure 6. *Ex* vivo study of basal cell carcinoma without immersion medium. An *ex vivo* study of basal cell carcinoma, imaged immediately after excision without immersion in any culture medium. The THz image is oriented to the visible image. The dotted white line indicates the axis of the vertical histology section. The white 'x' marks the location of the suture. The THz absorption profile is oriented to histology, where ✻ marks the tumour.

There is chronic intradermal inflammation in the area furthest from the suture. In the terahertz absorption profile, the increase in the TPP value correlates well with the location of tumor sites seen histologically, but interestingly absorption is less in areas of inflammation.

Sample 12 (**Fig 4*c***) is from a patient with a highly infiltrating tumor 25 × 15 mm, located on the chin. The visible image shows no obvious tumor and the normal tissue was marked with ink by the surgeon during reconstruction. In the terahertz image a very strong contrast is observed between the diseased and normal tissue. The diseased area, shown in red, covers two-thirds of the tissue, and is predominantly away from the suture. **Figure 5**(***c***) shows the histology and terahertz absorption profile. In the histology section, normal tissue is evident in the region closest to the suture. The remainder of the tissue is entirely diseased; the tumor extends to a depth of approximately 0.7 mm below the epidermis involving the subcutaneous fat and muscle. The terahertz absorption profile agrees well with histology, with a marked increase in the TPP value in the location of the tumor.

Table I summarizes the results from all 21 samples imaged. Four samples (6, 10, 16, 21) showed no increase in terahertz absorption and were identified as being no different statistically from normal tissue using TPI. Sample 6 was a re-excision of an apparently incompletely excised BCC, but histology confirmed no residual tumor. Samples 10, 16, and 21 were samples of normal tissue included by the surgeon as blind controls.

There were concerns that storage in culture medium may change or enhance the contrast in the terahertz images. A clinically well-defined BCC was excised from the right temple of a 92-y-old female patient and imaged within 5 min of surgery, without storage in keratinocyte culture medium. Similar patterns and levels of contrast were seen, as with all previous cases, and the terahertz contrast correlated well with histology (**Fig 6**). These findings indicate that the contrast observed is unlikely to have been influenced by the storage conditions.

DISCUSSION

The study describes the application of TPI for imaging BCC *ex vivo* over a region of the electromagnetic spectrum not investigated previously. The BCCs showed an increase in absorption of terahertz compared to normal tissue. The level of contrast observed in the terahertz images was sufficient to identify tumor margins when compared to histology. The source of this contrast, however, is still under investigation.

Recent studies have shown that the difference in the terahertz time-domain waveform between diseased and normal tissue is relatively narrow (Woodward *et al*, 2002). This narrow difference in time results in a broadband change in the frequency domain. Simple diatomic polar molecules, e.g., water, readily absorb terahertz radiation (Smye *et al*, 2001). Water has a strong broadband absorption around 6 THz, arising from the stretching of the hydrogen bond between molecules, the tail of which extends to the lower frequencies, with significant absorption in the operating

range of our TPI system (Thrane *et al*, 1995; Zelsmann *et al*, 1995). Increased water content in malignant tissues has been observed in many other different tumor types, and is commonly used as a marker for malignancy (Ross and Gordon, 1982; Chen *et al*, 1992; Rofstad *et al*, 1994).

Investigations in the mid-infrared between BCC and normal tissue have found BCCs to display reductions in the hydrogen bonding between functional groups of amino acids (Jeffrey, 1997). In malignant tissue significant fractions of the phosphate groups, originating mainly in phosphodiester groups of nucleic acids, were found to be hydrogen bonded, and the ratio of methyl (CH_3) to methylene (CH_2) was also found to decrease (Wong *et al*, 1993). Raman spectroscopy has shown that these changes may result from differences in the molecular structure of proteins and lipids between neoplastic and normal tissue (Gniadecka *et al*, 1997). The changes in absorption arising from vibrations within larger molecules, such as proteins, may be caused by a change in the hydrogen bonds between these larger functional groups and water molecules.

At NIR wavelengths between 1100 and 2500 nm, the absorptions arise from overtones and combination bands of the molecular vibrations of C–H, N–H, and O–H groups (McIntosh *et al*, 2001). Previous investigations of skin lesions using NIR spectroscopy have identified water to be a dominant feature in the identification of disease tissue, where a change in the amount or binding of water occurs between some types of lesions and control tissue (McIntosh *et al*, 1999; 2001). The major components of skin are proteins, proteoglycans, and water. The water is found either free or bound to the surface of proteins, like collagen. The observed increase in terahertz absorption is most probably due to either an increase in interstitial water within the diseased tissue (Lahtinen *et al*, 1999) or a change in the vibrational modes of water molecules with other functional groups.

Real-time *in vivo* stratum corneum thickness measurements on the palm of the hand, at a depth resolution comparable to OCT, have already been achieved using our TPI system (Cole *et al*, 2001). The lateral resolution of TPI is inferior to NIR techniques as a result of the diffraction limitation at longer wavelengths, but the technique does not suffer problems due to scatter. Near field transmission measurements using terahertz have already achieved lateral resolutions of 55 μm (Han *et al*, 2000). Improvements in terahertz generation and detection efficiency, and the development of TPI systems with greater bandwidths, are under way. These developments promise greater depth resolution and improved axial resolution, along with increased spectral content. The ability of TPI to differentiate tumor types and inflammation and to identify skin adnexae, such as sebaceous glands and hair follicles, is being investigated.

A pixel acquisition rate of 40 Hz is already possible, allowing for real-time line scanning using our system. Real-time imaging of an area using mechanical scanning does have its limitations. Others have shown that a CCD camera can be used to acquire spectral information incrementally over many pixels, however, which could reduce imaging time (Wu *et al*, 1996; Jiang and Zhang, 1998).

There is a need for a system to define the histologic subtypes of skin tumors, and determine subclinical margins preoperatively, to make MMS less time consuming and hence less expensive. Several promising imaging techniques are investigating dysplastic tissue and skin cancer, such as confocal microscopy and OCT. Both can provide high resolution detailed images but no technique has yet been able to identify tumor margins macroscopically without the use of image reconstruction. The ability to image tumors macroscopically using TPI allows a direct comparison between the terahertz and clinical images. The lateral and axial resolutions and the ability to image large areas up to 25×25 mm in less than 5 min is sufficient for TPI to play a role in identifying tumor margins. The current resolution of TPI may limit the detection of small tumors, however. TPI may potentially complement other techniques with better resolution, like confocal microscopy and OCT.

CONCLUSION

The results presented here demonstrate the ability of TPI to distinguish between BCC and normal tissue using the TPP analysis technique. This technique is the first to be used to identify BCC macroscopically in the terahertz frequency regime; it provides both structural information and chemical specificity. Of the 21 samples imaged, the 17 exhibiting BCC were successfully identified. For the remaining four samples no significant difference in contrast was observed in the terahertz images between the suspected diseased tissue and the normal skin, and the suspect tissues were all subsequently confirmed normal histologically. The increase in absorption observed in the diseased tissue may be attributed to either an increase in the interstitial water within the diseased tissue, or a change in the vibrational modes of water molecules with other functional groups. This makes water seem an important molecular marker for TPI. Our results represent a new application for the use of terahertz radiation in distinguishing carcinoma from normal tissue. Additional investigations are required to fully understand the source of this contrast and determine the role of TPI for tumor margin assessment.

We acknowledge EPSRC, TeraView Ltd., and Toshiba for their financial support. We are grateful to Dr. Ed Rytina, consultant dermatopathologist at Addenbrooke's Hospital, for reviewing the histology. TPI™ is a registered trademark of TeraView Ltd.

REFERENCES

American Cancer Society: *Cancer Facts and Figures.* Atlanta, GA: 2001

Arnone DD, Ciesla CM, Corchia A, *et al*: Application of terahertz (THz) technology to medical imaging. *Proc SPIE* 3823:209–219, 1999

Barlow RJ: *Statistics. A Guide to the Use of Statistical Methods in the Physical Sciences.* New York: John Wiley, 1989

Bushberg JT: *The Essential Physics of Medical Imaging.* Baltimore, MD: Williams & Wilkins, 1994

Chen JH, Avram HE, Crooks LE, Arakawa M, Kaufman L, Briton AC: *In vivo* relaxation times and hydrogen density at 0.063–4.85 T in rats with implanted mammary adenocarcinomas. *Radiology* 184:427–434, 1992

Clothier R: Personal correspondence, 2002

Cole BE, Woodward RM, Crawley D, *et al*: Terahertz imaging and spectroscopy of human skin, *in vivo. Proc SPIE* 4276:1–10, 2001

European Standard. Safety of Laser Products, 1994

Fornage BD, McGavran MH, Duvic M, Waldron CA: Imaging of the skin with 20 MHz US. *Radiology* 189:69–76, 1993

Gniadecka M, Wulf HC, Nielsen OF, Christensen DH, Hercogova J: Distinctive molecular abnormalities in benign and malignant skin lesions: studies by Raman spectroscopy. *Photochem Photobiol* 66:418–423, 1997

Han PY, Cho GC, Zhang XC: Time-domain transillumination of biological tissues with terahertz pulses. *Opt Lett* 24:242–244, 2000

Heinritz H, Benzel W, Hoffmann K, Iro H: Imaging superficial skin tumors of the ENT area. High frequency ultrasound in comparison with computerized tomography and magnetic resonance tomography. *HNO* 43:6–11, 1995

Hoffmann K, Stucker M, el-Gammal S, Altmeyer P: Digital 20 MHz sonography of basalioma in the B-scan. *Hautarzt* 41:333–339, 1990

Hoffmann K, Happe M, Schuller S, *et al*: Ranking of 20 MHz sonography of malignant melanoma and pigmented lesions in routine diagnosis. *Ultraschall Med* 20:104–109, 1999

Holme SA, Malinowsky K, Roberts DL: Changing trends in non-melanoma skin cancer in South Wales: 1988–98. *Br J Dermatol* 143:1224–1229, 2000

Huzaira M, Rius F, Rajadhyaksha M, Anderson RR, Gonzalez S: Topographic variation in normal skin, as viewed by *in vivo* reflectance confocal microscopy. *J Invest Dermatol* 116:846–852, 2001

Jeffrey GA: *An Introduction to Hydrogen Bonding*, 1st edn. New York: Oxford University Press, 1997

Jiang Z, Zhang XC: Single-shot spatiotemporal terahertz field imaging. *Opt Lett* 23:114–116, 1998

Kuranov RV, Sapozhnikova VV, Tuchin IV, Zagainova E, Gelikonov VM, Kamemsky VA: Complementary use of cross-polarisation and standard OCT for differential diagnosis of pathological tissue. *Optics Express* 10:707–713, 2002

Lahtinen T, Nuutinen J, Alanen E, Turunen M, Nuortio L, Usenius T, Hopewell JW: Quantitative assessment of protein content in irradiated human skin. *Int J Radiat Oncol Biol Phys* 43:635–638, 1999

Lassau N, Spatz A, Avril MF, *et al*: Value of high-frequency US for preoperative assessment of skin tumors. *Radiographics* 17:1559–1565, 1997

McIntosh LM, Summers R, Jackson M, *et al*: Infrared spectra of basal cell carcinomas are distinct from non-tumor-bearing skin components. *J Invest Dermatol* 112:951–956, 1999

McIntosh LM, Summers R, Jackson M, *et al*: Towards non-invasive screening of skin lesions by near-infrared spectroscopy. *J Invest Dermatol* 116:175–181, 2001

Price RR: The AAPM/RSNA physics tutorial for residents. MR imaging safety considerations. Radiological Society of North America. *Radiographics* 19:1641–1651, 1999

Rajadhyaksha M, Zavislan JM: Confocal reflectance microscopy of unstained tissue *in vivo*. *Retinoids* 14:26–30, 1998

Rajadhyaksha M, Grossman M, Esterowitz D, Webb RH, Anderson RR: *In vivo* confocal scanning laser microscopy of human skin: melanin provides strong contrast. *J Invest Dermatol* 104:946–952, 1995

Rajadhyaksha M, Menaker G, Flotte T, Dwyer PJ, Gonzalez S: Confocal examination of nonmelanoma cancers in thick skin excisions to potentially guide Mohs micrographic surgery without frozen histopathology. *J Invest Dermatol* 117:1137–1143, 2001

Rapini RP: Comparison of methods for checking surgical margins. *J Am Acad Dermatol* 23:288–294, 1990

Rofstad EK, Steinsland E, Kaalhus O, Chang YB, Hovik B, Lyng H: Magnetic resonance imaging of human melanoma xenografts *in vivo*: proton spin lattice and spin–spin relaxation times versus fractional water content and fraction of necrotic tumour tissue. *Int J Radiat Biol* 65:387–401, 1994

Ross KF, Gordon RE: Water in malignant tissue, measured by cell refractometry and nuclear magnetic resonance. *J Microscopy* 128:7–21, 1982

Schmitt JM, Yadlowsky MJ, Bonner RF: Subsurface imaging of living skin with optical coherence microscopy. *Dermatology* 191:93–98, 1995

Shriner DL, McCoy DK, Goldberg DJ, *et al*: Mohs' micrographic surgery. *J Am Acad Dermatol* 39:79–97, 1998

Smye SW, Chamberlain JM, Fitzgerald AJ, Berry E: The interaction between terahertz radiation and biological tissue. *Phys Med Biol* 46:R101–R112, 2001

Song HK, Wehrli FW, Ma J: *In vivo* MR microscopy of the human skin. *MRM* 37:185–191, 1997

Telfer NR, Colver GB, Bowers PW: Guidelines for the management of basal cell carcinoma. *Br J Dermatol* 141:415–423, 1999

Thrane L, Jacobsen RH, Uhd Jepsen P, Keiding SR: THz reflection spectroscopy of liquid water. *Chem Phys Lett* 240:330–333, 1995

Van Exter M, Grischkowsky DR: Characterization of an optoelectronic terhertz beam. *IEEE Trans Microwave Theory Tech* 38:1684–1691, 1990

Wolf DJ, Zitelli JA: Surgical margins for basal cell carcinoma. *Arch Dermatol* 123:340–344, 1987

Wong PT, Goldstein SM, Grekin RC, *et al*: Distinct infrared spectroscopic patterns of human basal cell carcinoma of the skin. *Cancer Res* 53:762–765, 1993

Woodward RM, Wallace VP, Cole BE, *et al*: Terahertz pulse imaging in reflection geometry of skin tissue using time domain analysis techniques. In: Cohn GE, ed. *Clinical Diagnostic Systems: Technologies and Instrumentation, Proc SPIE*, 4625, 160–169, 2002

Wu QT, Zhang XC: Free-space electro-optic sampling of terahertz beams. *Appl Phys Lett* 67:3523–3525, 1995

Wu QT, Hewitt TD, Zhang XC: Two-dimensional electro-optic imaging of THz beams. *Appl Phys Lett* 69:1026–1028, 1996

Zelsmann HR: Temperature dependence of the optical constants for liquid H_2O and D_2O in the far IR region. *J Mol Struc* 350:95–114, 1995